JOURNAL OF MATERIALS SCIENCE 14 (1979) 776–788

Interaction of lattice dislocations with periodic grain boundary structures

W. A. T. CLARK*, D. A. SMITH
Department of Metallurgy and Science of Materials, University of Oxford, Parks Road, Oxford, UK

Some recent discussions have centred on the mechanism by which lattice dislocations are absorbed by grain boundaries at high temperatures. Boundaries in two well-characterized coincidence site lattice systems have been studied using an electron microscope hot stage. The dislocation behaviour was shown to be consistent with a description based on dissociation and reactions involving grain boundary dislocations. A model of grain boundary migration based on the motion of grain boundary dislocations depends on both the boundary crystallography and the temperature, and may account for experimental measurements of grain boundary migration activation volumes.

1. Introduction

During recrystallization grain boundaries migrate and absorb the dislocations which are produced during cold working. Hot-stage transmission electron microscopy of the migration and grain boundary interactions with dislocations may help to elucidate the mechanisms of these processes. Earlier work by Pumphrey and Gleiter [1, 2] indicates that a dislocation is absorbed by high angle grain boundaries with an associated cancelling of the long-range elastic field, since the discrete lattice dislocation image broadens, decreases in intensity, and ultimately disappears. Pond and Smith [3, 4] suggest that the absorption process can be described in terms of dislocation dissociation and reactions appropriate to the structure of the particular grain boundary. In order to distinguish one mechanism from another, it is necessary to use a range of well-defined systems. In this paper the interaction of crystal lattice dislocations with two coincidence related boundaries in annealed stainless steel is described.

2. Experimental techniques

2.1. Specimen preparation

The material used in this investigation is an austenitic stainless steel conforming to the specification AISI 316, and having nominal composition 17.5% Cr–9.8% Ni–2.6% Mo–1.9% Mn–0.5% Si–0.1% C with the balance Fe. Initially received as rolled sheet of 250 μm thickness, it was annealed in vacuo for 15 min at 1050° C and quenched, producing a grain diameter of 30 to 40 μm. Thin foils for examination in the electron microscope were obtained by electropolishing in a solution of 10% perchloric acid/ethanol at 11 V d.c. and −25° C.

The specimens were examined in a JEOL 100C microscope operating at 100 kV, and fitted with a double tilt side-entry stage, in which the analysis of the grain boundary dislocation network was performed. The heating experiments were conducted in a Philips EM300, also operating at 100 kV, using a single tilt side-entry heating stage.

2.2. Hot stage operation

The experimental procedure adopted was as follows. The foil was heated at a chosen temperature for between 2 and 5 minutes; the image was studied during this time for modifications to the structure. To take micrographs the foil was cooled rapidly to room temperature, the image allowed to stabilize, and the plates exposed. This not only avoided the necessity to hold the specimen at an elevated temperature long enough

*Present address: Department of Metallurgical Engineering, Michigan Technical University, Houghton, MI 49931, USA.

TABLE I

T(° C)	D_b(m² sec^{-1})	$\sqrt{(Dt)}$(Å)	τ (sec)
1050	1.52×10^{-11}	1.17×10^{6}	6.57×10^{-4}
500	9.82×10^{-17}	2.97×10^{3}	1.02×10^{2}
20	3.46×10^{-37}	1.76×10^{-7}	2.89×10^{22}

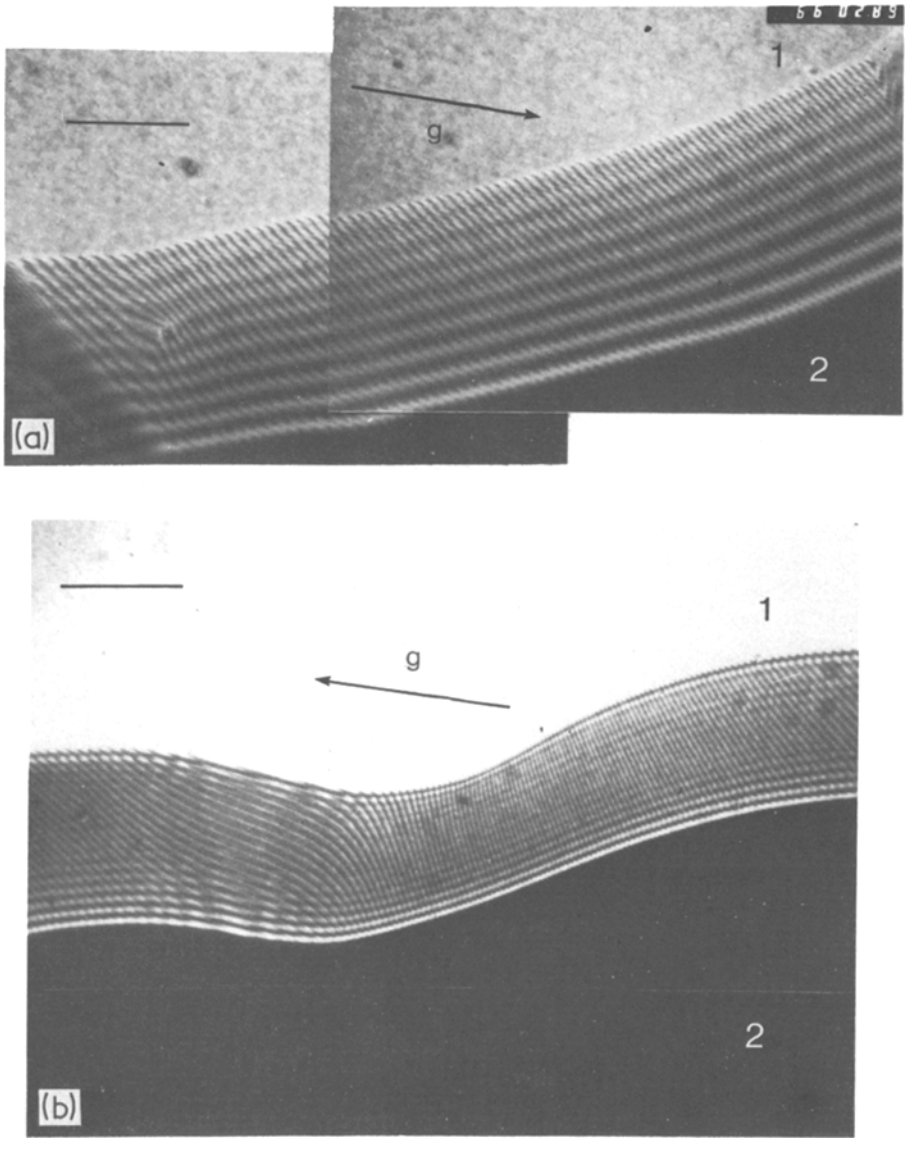

Figure 1 Different areas of the same $\Sigma = 31$ related boundary; note the strong contrast of the $\mathbf{b}_{31}$ type DSC dislocation referred to in the text. (a) $\mathbf{g} = 1\,1\,1_1$, dark-field (DF); (b) $\mathbf{g} = \bar{1}\,\bar{1}\,\bar{1}_1$, DF. Scale marker is 2500 A.

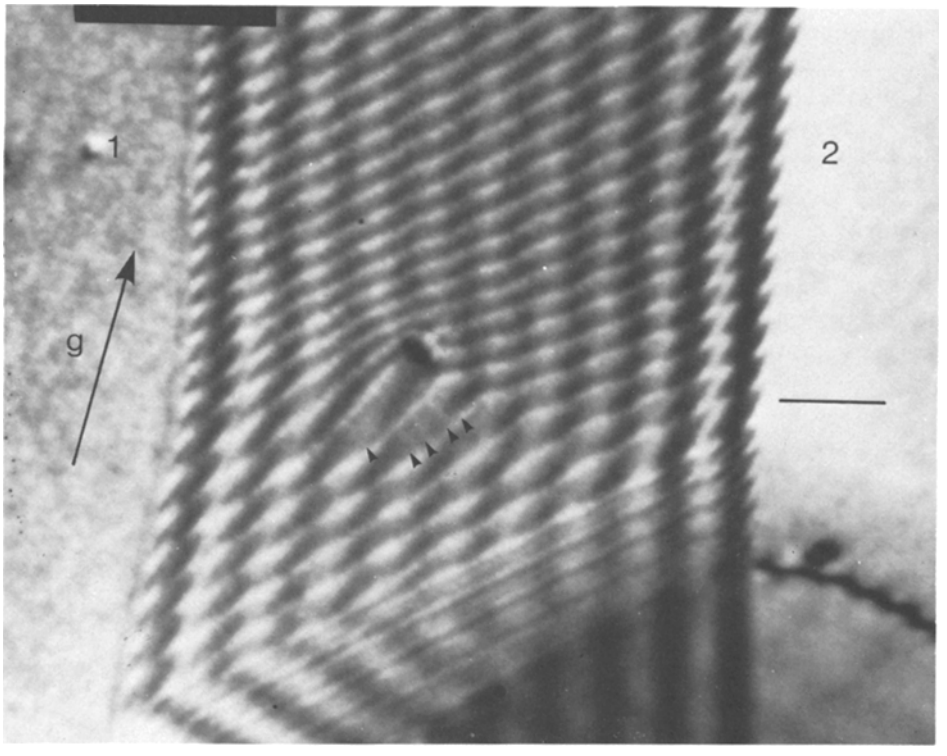

Figure 2 Enlargement of area around precipitate visible in Fig. 1a. The $\mathbf{b}_1$ or $\mathbf{b}_2$ dislocations (arrowed) are made visible by the change in their spacing resulting from the distortion of the boundary plane by the precipitate. $\mathbf{g} = 1\,1\,1_{1/2}$, bright-field (BF). Scale marker 1000 A

to eliminate specimen drift, but also minimized the reduction in image intensity due to thermal diffuse scattering. Since the hot stage has only a single tilt facility, the choice and control of diffracting conditions is severely restricted.

2.3. The rate of dislocation absorption

Little dislocation motion, or boundary migration, could be observed in this material until the hot stage temperature was above 500° C. At 550° C the first evidence of boundary migration was observed; due to the presence of the foil surfaces this was principally a rotation of the boundary to minimize its area and not representative of bulk behaviour. In order for complete absorption of crystal dislocations into the interface to take place, climb is generally necessary and dislocation movement in the boundary is then diffusion controlled. As the activation energy, Q, for boundary diffusion in stainless steel is $184\,\mathrm{kJ\,mol^{-1}}$ [5], the grain boundary diffusion coefficient, D_b, is

$$D_b = D_0 \exp(-Q/RT) \qquad (1)$$

where D_0 is $3 \times 10^{-4}\,\mathrm{m^2\,sec^{-1}}$ for a boundary width of 5 Å. Ignoring the possible modification of the diffusion coefficient as a result of interfacial dislocations acting as paths for pipe diffusion, the diffusion distance, equal to $\sqrt{(Dt)}$, is calculated for $t = 900$ sec (the heat-treatment time) at the annealing temperature (1050° C), room temperature (20° C), and a typical microscope hot stage temperature (500° C). The results are shown in Table I; τ is the time required for a random walk over a distance of 1000 Å.

It is reasonable to suppose that quenched-in boundary configurations are retained, even though they may not represent the equilibrium state of the interface. At the annealing temperature, however, dislocation absorption is extremely rapid.

3. Observations of coincidence related boundaries

3.1. The $\Sigma = 31$ interface

3.1.1. Crystallographic details

The interface shown in Fig. 1 is between two crystals misoriented by 17.43° (±0.06°) about an

axis [57 54 62] indexed with respect to crystal 1, and the grain boundary dislocation structure visible is interpreted in terms of a deviation of $1.22°/[\bar{1}\bar{1}\,45\,19]_1$ from the exact $\Sigma = 31$* coincidence disorientation generated by a rotation of 17.90° about the $[1\,1\,1]_{1/2}$ axis of the two crystals. The coincidence site lattice (CSL) cell is rhombohedral, and, as with other rhombohedral CSL cells produced by ⟨1 1 1⟩ rotations, the area density of coincidence sites on the various lattice planes is relatively isotropic. There are, therefore, several planes of the CSL with similar densities of coincidence sites, and it is this property which has been proposed [6] to account for the importance of the $\Sigma = 7$ boundary in recrystallization textures, by reducing the variation of boundary structure with orientation of the boundary plane. The interface plane was found to lie within ±4.0° of the $(3\,\bar{3}\,2)_1/(2\,\bar{3}\,3)_2$ plane.

3.1.2. Burgers vector determination

Image contrast invisibility experiments showed the grain boundary dislocations visible in Fig. 1 to have Burgers vectors most consistent with

$$a/31[9\,8\,14]_1 : a/31[8\,9\,14]_2$$

which are $\mathbf{b}_3$ type dislocations obtained from the DSC lattice [7] for the $\Sigma = 31$ system. These dislocations are consistent in orientation and spacing with the angular deviation from exact coincidence given above. Two further equivalent $\mathbf{b}_3$ type DSC vectors exist in this system and are

$$\mathbf{b}_{32} = a/31\,[14\,9\,8]_1 : a/31[14\,8\,9]_2$$

$$\mathbf{b}_{33} = a/31\,[8\,14\,9]_1 : a/31[9\,14\,8]_2$$

Other DSC dislocations with small Burgers vectors, were also visible in certain favourable diffracting conditions (Fig. 2), but may not be seen in Fig. 1. They have Burgers vectors

$$\mathbf{b}_1 = a/62[5\,1\,\bar{6}]_1 : a/62[6\,\bar{1}\,\bar{5}]_2 \quad \text{and}$$

$$\mathbf{b}_2 = a/62[1\,\bar{6}\,5]_1 : a/62[\bar{1}\,\bar{5}\,6]_2$$

It is clear that these grain boundary dislocations cannot by themselves account for the change in interface orientation observed in Fig. 1 since their density is much too low. It is necessary for this change to be accommodated either by finely spaced $\mathbf{b}_1$ and $\mathbf{b}_2$ type dislocations not resolved on the micrographs, or by the boundary microfaceting onto other planes.

3.1.3. Hot stage studies and dislocation absorption

Fig. 3 shows a series of micrographs of the boundary taken after the treatments indicated in the captions. The following observations are made. The first sign of boundary migration appeared after heating for one minute at 550° C (Fig. 3a), and this took the form of rotation of the boundary plane to realign perpendicular to the foil surface. Surface oxide particles appear, and these are differentiated from second phase particles forming in the foil. After two further minutes, at 600° C, isolated lattice dislocations, A, are seen approaching the boundary from crystal 1 (Figs. 3c and d); as they are visible in the common $g = 1\,1\,1_{1/2}$, their likely Burgers vector is $a/2[0\,1\,1]_1$, $a/2[1\,1\,0]_1$, or $a/2[1\,0\,1]_1$. The slip plane orientation and line direction in the boundary indicate that the dislocations lie on the $(1\,\bar{1}\,\bar{1})_1$ plane and thus have Burgers vector $a/2[1\,0\,1]_1$ or $a/2[1\,1\,0]_1$. The reactions for the dissociation of these dislocations into appropriate primitive DSC dislocations are

$$a/2[1\,1\,0]_1 \rightarrow \underset{\mathbf{b}_1}{a/62[5\,1\,\bar{6}]_1} + 2\cdot \underset{-\mathbf{b}_2}{a/62[\bar{1}\,6\,\bar{5}]_1} + \underset{\mathbf{b}_{32}}{a/31[14\,9\,8]_1} \tag{2}$$

and

$$a/2[1\,0\,1]_1 \rightarrow 3\cdot \underset{3\mathbf{b}_2}{a/62[1\,\bar{6}\,5]_1} + \underset{\mathbf{b}_{32}}{a/31[14\,9\,8]_1} \tag{3}$$

both of which involve the production of a $\mathbf{b}_3$ type DSC dislocation different from that observed in the network. The two $\mathbf{b}_3$ Burgers vectors lie only ~25° apart and both have a large component parallel to the $[1\,1\,1]_{1/2}$ rotation axis, so that the $\mathbf{b}_{32}$ dislocation is expected to align parallel to the existing network and show similar contrast in the diffracting conditions used in the hot-stage study. Suppose, for illustration, that the dislocations are taken to have the Burgers vector $a/2[1\,1\,0]_1$; the reaction with the $\mathbf{b}_3$ dislocations in the network (Figs. 3e and f) may be studied by means of the 0-lattice method [8].

*Σ is the reciprocal of the fraction of coincidence sites.

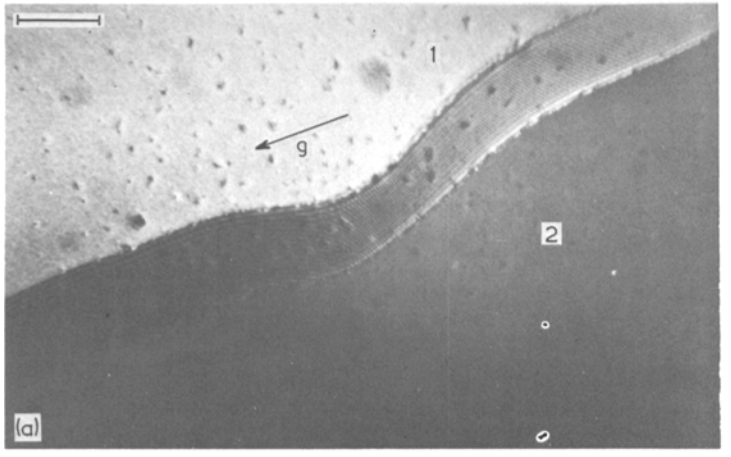
1
g
2
(a)

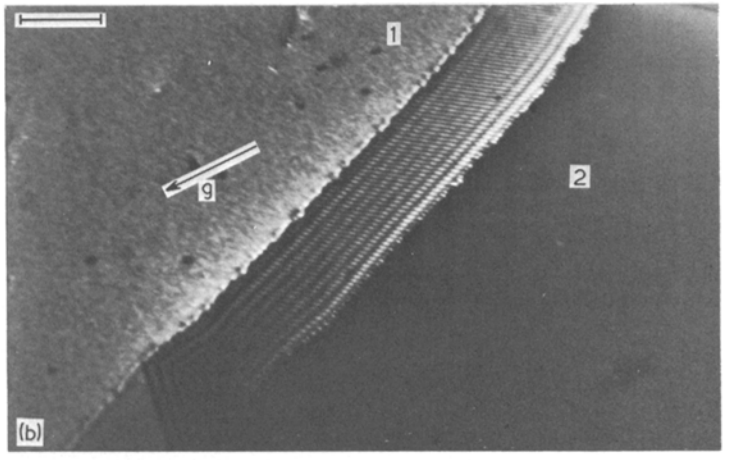
1
g
2
(b)

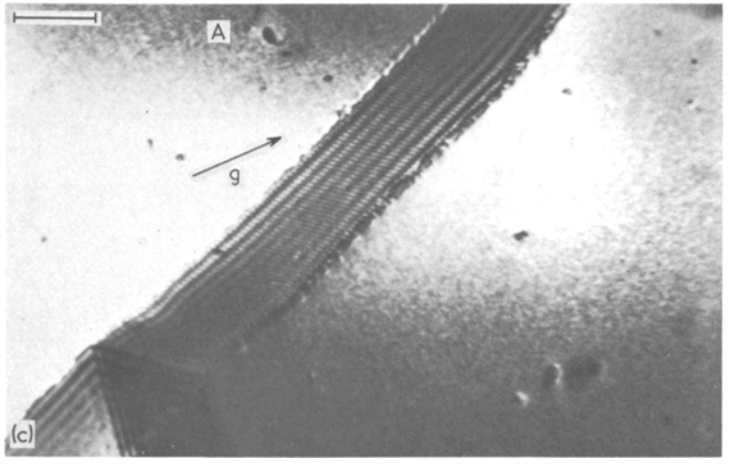
A
g
(c)

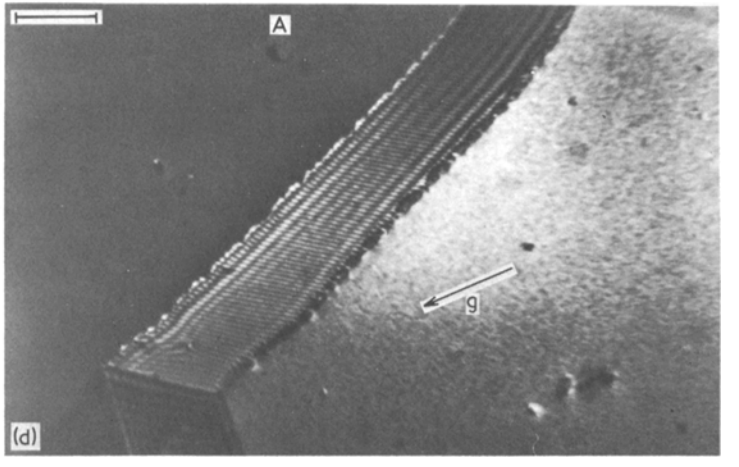
A
g
(d)

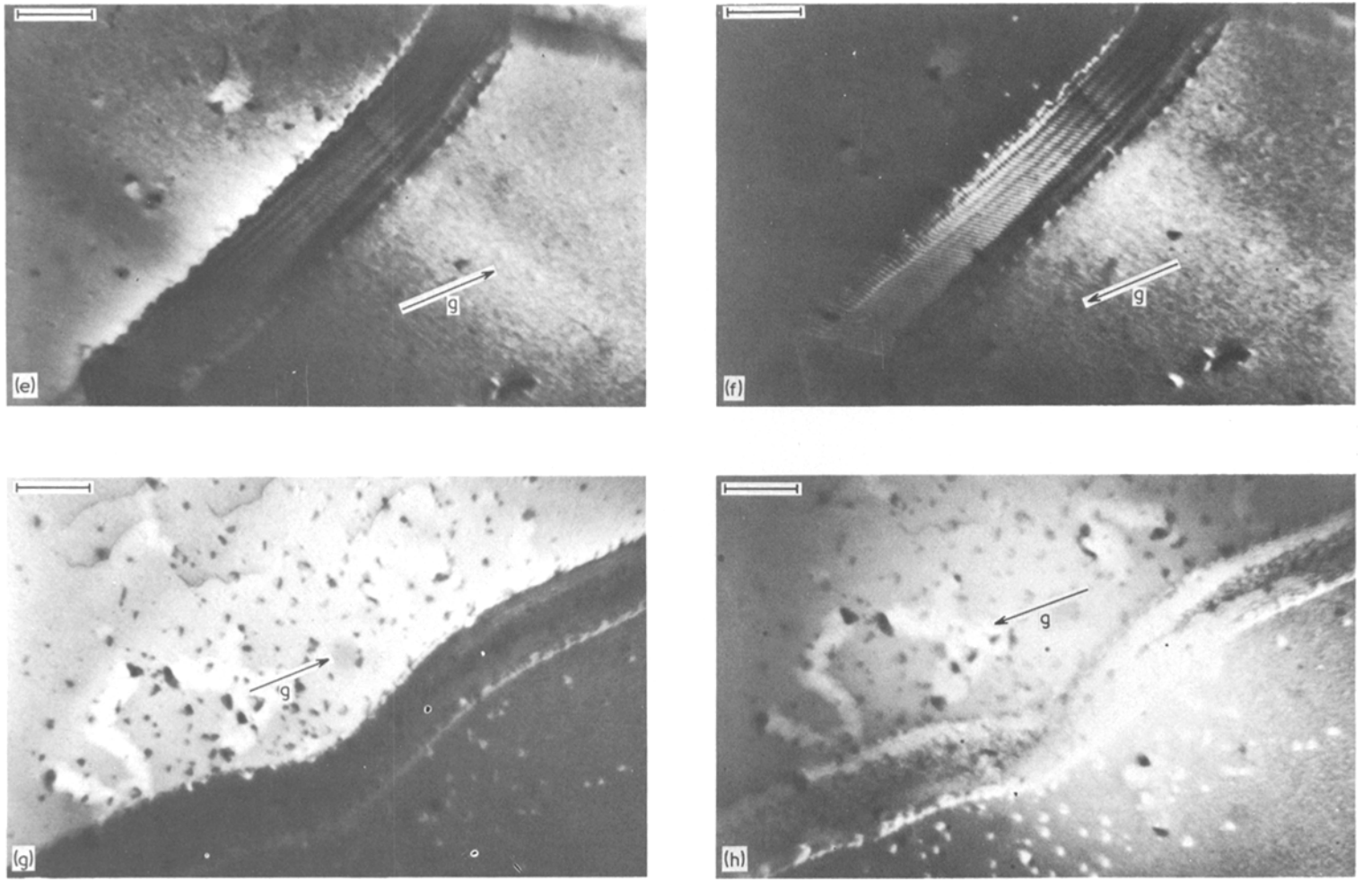

Figure 3 Heating stage observations of $\Sigma = 31$ related boundary. (a) After 60 sec at 550° C, $g = \bar{1}\,\bar{1}\,\bar{1}_{1/2}$; (b) after further 60 sec at 575° C, $g = \bar{1}\,\bar{1}\,\bar{1}_{1/2}$. After a further 2 min at 600° C: (c) $g = 1\,1\,1_{1/2}$ BF; (d) $g = 1\,1\,1_{1/2}$ DF. A further 2 min at 625° C: (e) $g = 1\,1\,1_{1/2}$ BF; (f) $g = \bar{1}\,\bar{1}\,\bar{1}_{1/2}$ DF. Note the absorption of the dislocation into the boundary. A further 2 min at 750° C: (g) $g = 1\,1\,1_{1/2}$ BF; (h) $g = \bar{1}\,\bar{1}\,\bar{1}_{1/2}$ DF. Rotation of the boundary plane and profuse oxidation are observed. Scale marker 2500 Å.

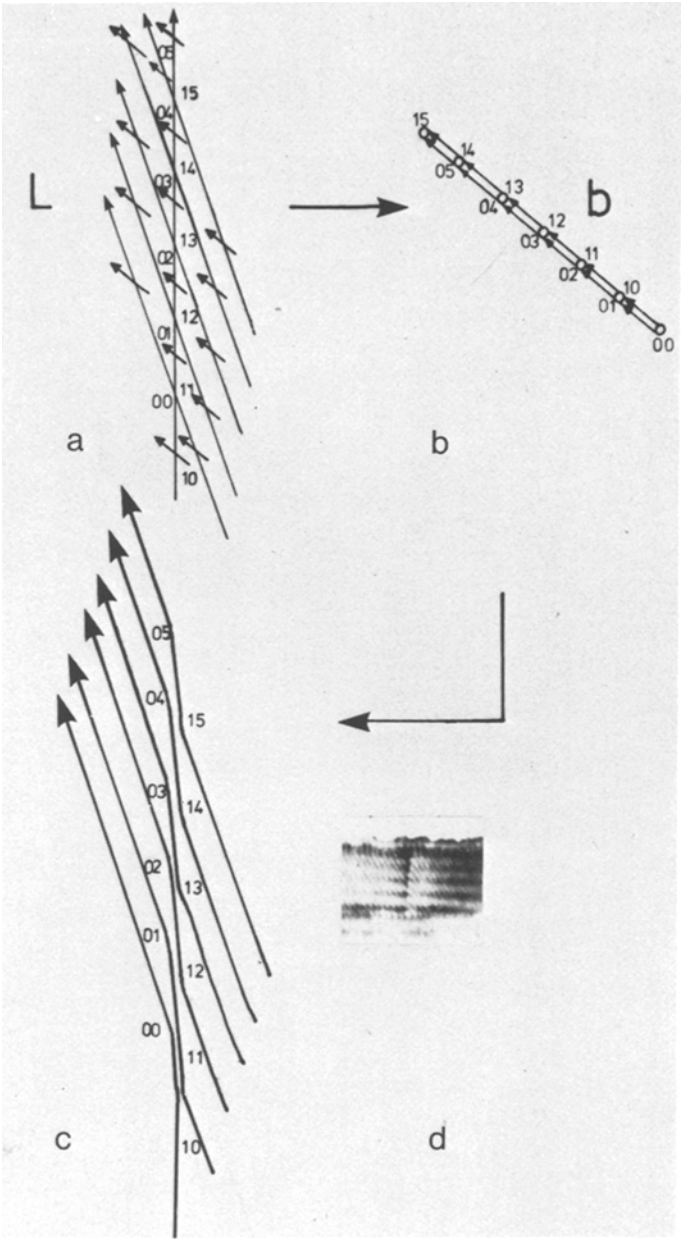

Figure 4 The construction used to study the interaction of the crystal lattice dislocation with the $\mathbf{b}_{31}$ DSC dislocations in the boundary. (a) The original L-net with lattice dislocation superimposed; (b) is the *b*-net representing this configuration which leads to (c), the modified L-net, which is compared to the inset of the boundary (d).

Fig. 4 shows the construction required; the L-space contains the dislocations with line direction $[6\,8\,3]_1$ in the boundary plane. The incoming dislocation is assumed to dissociate by the reaction given above, and the $\mathbf{b}_1$ and $\mathbf{b}_2$ components have a Burgers vector too small to be resolved in the image, and are not considered in the diagram. The line direction of the lattice dislocation is $[1\,1\,0]_1$, which lies 18.5° from the line of the grain boundary dislocations. The *b*-space contains the Burgers vectors, and it may be seen from the labelling of the L-fields, and the application of the duality relations [8], that there are places in the *b*-net where the merging of certain Burgers vectors occurs, so that two numbers are attributed to the same *b*-node. Hence the corresponding L-fields are continuous, which leads to the configuration of Fig. 4c, which may be directly compared with Fig. 4d. A similar process would occur for the $a/2[1\,0\,1]_1$ dislocation.

3.1.4. Mechanisms of dislocation image broadening

Reactions 2 and 3 demonstrate a mechanism by which lattice dislocations interacting with a grain boundary may be absorbed into the existing grain boundary dislocation network, and thus lose their distinct character in their image. Pumphrey and Gleiter [1, 2] recently discussed the absorption of crystal lattice dislocations into so-called "random" boundaries (i.e. boundaries whose misorientation was not close to any low-Σ coincidence system), in which the arriving dislocation shows a broader image in the boundary than in the crystal, this image gradually disappearing on heating the specimen. The interpretation of this observation as indicating that a dislocation is able to "spread its core" in the boundary plane by a relaxation along the interface may be compared to the above reaction, and the following points noted.

Firstly, consider the dislocation network to be made up of $\mathbf{b}_1$ and $\mathbf{b}_2$ type DSC dislocations only, as would be the case if the $\mathbf{R}(02)$ axis [9] were parallel to the rotation axis for the coincidence misorientation. If the incoming lattice dislocation also has a Burgers vector lying in this zone (e.g. $a/2[0\,1\,\bar{1}]_1$ in this case) the dissociation of the lattice dislocation in the boundary would be of the form:

$$a/2[0\,1\,\bar{1}]_1 \rightarrow \underset{\mathbf{b}_1}{a/62[5\,1\,\bar{6}]_1} + \underset{5\mathbf{b}_2}{5a/62[\bar{1}\,6\,\bar{5}]_1} \qquad (4)$$

with no $\mathbf{b}_3$ dislocation produced. The product dislocations would then move apart under their mutual repulsion, requiring diffusion to take place unless the boundary plane is $(1\,1\,1)_{1/2}$. The separation of the dislocations is then governed by the rate of diffusion in the interface, which is in turn a function of the temperature. As has already been shown for a material such as stainless steel, the diffusion rate is so low at room temperature that the dislocations are unlikely to move an appreciable distance apart, and thus will show the image characteristics of their total Burgers vector. However, should the temperature be increased sufficiently to permit diffusion to take place rapidly, the accommodation of the dislocation into the boundary could proceed, and the final configuration would contain a regularly spaced array of $\mathbf{b}_1$ and $\mathbf{b}_2$ type dislocations. For such an interface, as the micrographs have indicated, this network is unlikely to be resolved and the lattice dislocation image will have "disappeared" in the boundary.

An intermediate stage of the process will require that an area of the boundary contains a higher density of grain boundary dislocations than at the equilibrium spacing; strong-beam electron diffraction will be unable to resolve the individual dislocations if the spacing is $\sim\frac{1}{3}\xi g$ or less [10], and the dislocation image will appear to have "spread" in the micrograph. The final disappearance of the dislocation image does not, however, necessarily indicate that DSC type dislocations are not being produced in the boundary, and no periodic pattern maintained, even for cases where the CSL and DSC lattice are anisotropic; only the accurate determination of all the grain boundary parameters can ascertain the precise reaction, and hence the image behaviour expected.

It must also be remembered that the physical integrity of individual grain boundary dislocations may extend to separations ($4a$ to $5a$, where a is the lattice parameter) below the resolution of current electron microscope techniques for their examination (20 Å for $a/6\langle 1\,1\,2\rangle$ dislocations in weak-beam microscopy–greater for smaller Burgers vectors), and that care must be taken to distinguish the limitations of electron diffraction from those of grain boundary dislocation models.

It is observed that the $\mathbf{b}_3$ type dislocations remain visible throughout the heating, but are confined to the boundary plane. Subsequent micrographs indicate that although extensive surface oxidation, and rotation of the boundary plane occur (Figs. 3g and h), and $\mathbf{b}_3$ dislocation images persist, but are not observed to move along the boundary plane, as boundary migration might require.

3.2. The $\Sigma = 9$ interface

3.2.1. Crystallography and Burgers vector determination

A further boundary was examined in which the misorientation was $154.30° (\pm 0.20°)/[\bar{4}\bar{7}\,\bar{4}\bar{7}\,\bar{6}\bar{9}]_1$, that is a deviation of $1.61°/[1\,4\,4]_1$ from $152.73°/[\bar{2}\,\bar{2}\,\bar{3}]_{1/2}$, one of the alternative descriptions of the $38.94°/[0\,\bar{1}\,\bar{1}]_1\,[\bar{1}\,0\,\bar{1}]_2$ $\Sigma = 9$ disorientation. In this case three components of a grain boundary dislocation network were resolved – these are labelled A, B, and C in Fig. 5. The Burgers vectors were again determined and are

$$A\,(\mathbf{b}_1) = a/18[4\,\bar{1}\,1]_1 : a/18[\bar{1}\,\bar{4}\,1]_2$$

$$B\,(\mathbf{b}_2) = a/9[1\,2\,\bar{2}]_1 : a/9[\bar{2}\,\bar{1}\,2]_2$$

$$C\,(\mathbf{b}_3) = a/18[1\,2\,7]_1 : a/6[2\,1\,1]_2$$

Three other equivalent $\mathbf{b}_3$ type Burgers vectors are found in the $\Sigma = 9$ system and are

$$\mathbf{b}_{32} = a/6[1\,2\,1]_1 : a/18[2\,1\,7]_2$$

$$\mathbf{b}_{33} = a/6[\bar{1}\,1\,2]_1 : a/18[\bar{1}\,\bar{1}\,2]_2$$

$$\mathbf{b}_{34} = a/18[\bar{1}\,7\,2]_1 : a/6[1\,\bar{1}\,2]_2$$

The boundary plane was within ±4° of $(2\,2\,3)_{1/2}$.

3.2.2. Hot stage studies and dislocation absorption

The hot stage experiments were carried out in the same manner as in the previous example. After one minute at 575° C the broad image of the lattice dislocations in crystal 1($\mathbf{b} = a/2[1\,\bar{1}\,0]_1$) (Fig. 5a) was seen to have almost disappeared, presumably by dissociation of the dislocation by a reaction such as

$$a/2[1\,\bar{1}\,0]_1 \rightarrow 2a/18[4\,\bar{1}\,1]_1 + a/18[1\,\bar{7}\,\bar{2}] \qquad (5)$$

$$2\mathbf{b}_1 \qquad -\mathbf{b}_{34}$$

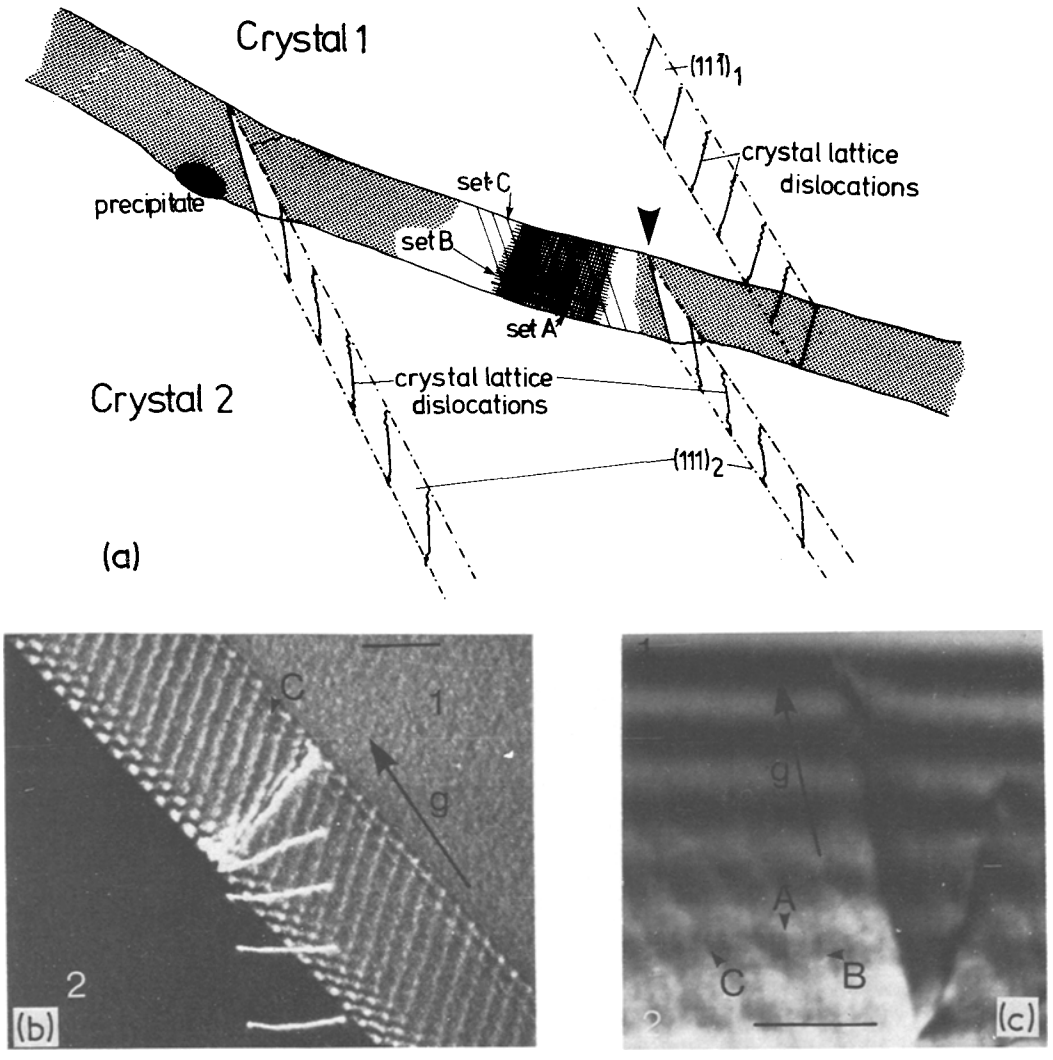

Figure 5 Sketch and micrographs of the $\Sigma = 9$ related boundary. The grain boundary dislocations are labelled on the micrographs, which show the interaction of the boundary and the pile-up of crystal lattice dislocations from crystal 2 (shown arrowed in (a)). (b) $\mathbf{g} = 1\,1\,\bar{3}_1/\bar{3}\,\bar{1}\,1_2$ DF; (c) $\mathbf{g} = 2\,0\,0_2$ BF. Scale marker is 1000 A.

The residual image is shown in Figs. 6a and b, where it is observed that the portion of lattice dislocation not so far absorbed is protruding from the interface. The faint trace visible along the previous dislocation line is comparable in contrast to the $\mathbf{b}_3$ type dislocations in the boundary, which is taken as further evidence for the validity of the interpretation in terms of dissociation. The same area is also shown in Figs. 6c and d. In Fig. 6c the $\mathbf{b}_1$ type array is visible, in the background, while in Fig. 6d the single interacting dislocation appears to dissociate into at least two resolvable dislocations, as the reaction 5 predicts. Finally, Figs. 6e and f image only the $\mathbf{b}_1$ type dislocations; thus it is shown that both the $\mathbf{b}_1$ and $\mathbf{b}_3$ dislocations persist in the interface during migration, whereas the discrete image of the crystal lattice dislocation absorbed into the boundary disappears.

The observations presented are further evidence that (i) certain high angle grain boundaries contain regular networks of dislocations with Burgers vectors of the DSC lattice [7], and (ii) such boundaries are capable of absorbing crystal lattice dislocations by dissociating them into grain boundary dislocations and incorporating them into the existing interfacial structure; the rate of the incorporation depends on the temperature.

4. Boundary migration by dislocation motion

It is then reasonably easy to envisage how, in a process such as recrystallization, an advancing boundary may absorb lattice dislocations produced in cold-working and leave an essentially dislocation-free crystal behind it. The absorbed dislocations will modify the grain boundary dislocation network and may change the migration rate of the interface. Consider, for example, two fcc crystals which are twinned with respect to one another. The glide of an $a/6[\bar{2}\,1\,1]$ partial across the (1 1 1) twin plane moves the boundary by one (1 1 1) planar spacing in a direction dependent on the direction of motion and Burgers vector of the partial, and the growth of one crystal with respect to the other could be achieved without diffusion taking place. Fig. 7a shows the analogous situation in the $\Sigma = 9$ misorientation studied in Section 3.2. The boundary plane is chosen in this case to be one of the twin interfaces for this system, $(1\,2\,\bar{2})_1/(\bar{2}\,\bar{1}\,2)_2$, and the DSC lattice is taken as the reference lattice for the Burgers circuit. An edge grain boundary dislocation with a $\mathbf{b}_1$ Burgers vector, $a/18[4\,\bar{1}\,1]_1$; $a/18[\bar{1}\,4\,1]_2$ is seen as two extra $(8\,\bar{2}\,2)_1$ planes visible in crystal 1, and is moving from left to right of the diagram. It is clearly seen that the shift of the boundary plane normal to the interface is equal to the shift of the CSL unit cell in the same direction, and the boundary migrates from crystal 1 into crystal 2, by an amount $a/9[\bar{1}\,\bar{2}\,2]_1$ or 0.33 units of a. This is once again accomplished by glide alone.

Fig. 7b shows the same crystals in the same misorientation, but with the other twin plane as boundary plane $(4\,\bar{1}\,1)_1/(\bar{1}\,4\,1)_2$. The same dislocation is considered, but is now seen to form a sessile edge at the boundary, with its Burgers vector perpendicular to the boundary plane. The dislocation is now restricted to move by climb only, and diffusion of material to and from the interface is necessary, with the boundary position remaining unaltered. For a tilt boundary plane intermediate between these two positions, the motion of the $\mathbf{b}_1$ dislocation will necessitate both glide and climb, the relative contribution of each being a function of the boundary plane orientation. Therefore different interface planes separating the same two crystals may migrate at different rates, and the activation volume for boundary migration may also vary with boundary plane. Haessner [11] indicates that observed activation volumes are more typical of group processes associated with the movement of several atoms, rather than single atoms as might be anticipated if migration were considered to be the simple diffusion of single atoms across the boundary from sites in crystal 1 to sites in crystal 2. The combination of glide and climb necessary in general to accomplish boundary migration by the passage of DSC dislocations is compatible with this idea, as a small amount of climb of the extra half planes of the dislocation may enable a considerable amount of glide, and hence boundary movement, to take place.

5. Concluding remarks

Crystal lattice dislocations interacting with grain boundaries may dissociate into the appropriate DSC dislocations which may then move in the boundary at a rate dependent on the orientation of the Burgers vectors and the temperature. This

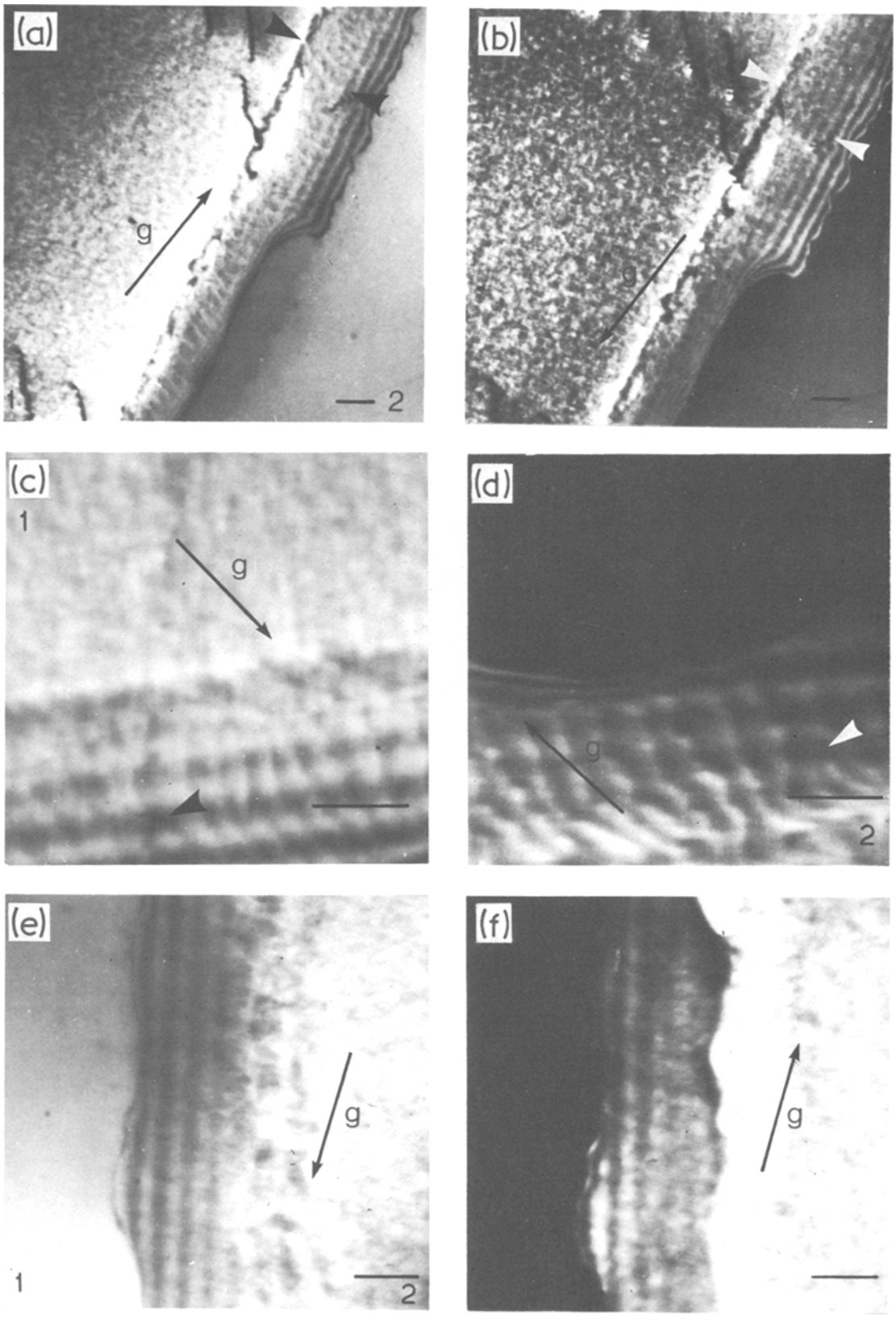
(a)
g
1
2
(b)
g
(c)
1
g
(d)
g
2
(e)
g
1
2
(f)
g

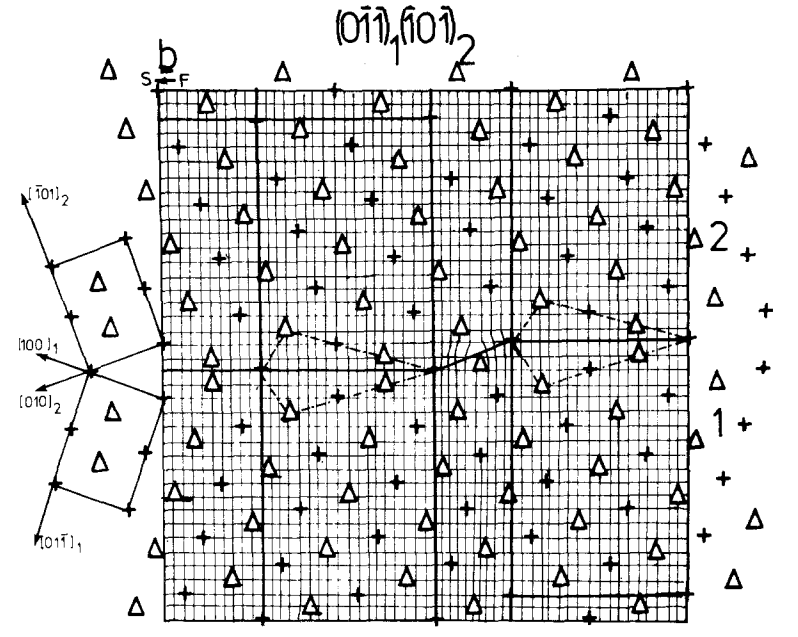

(a)

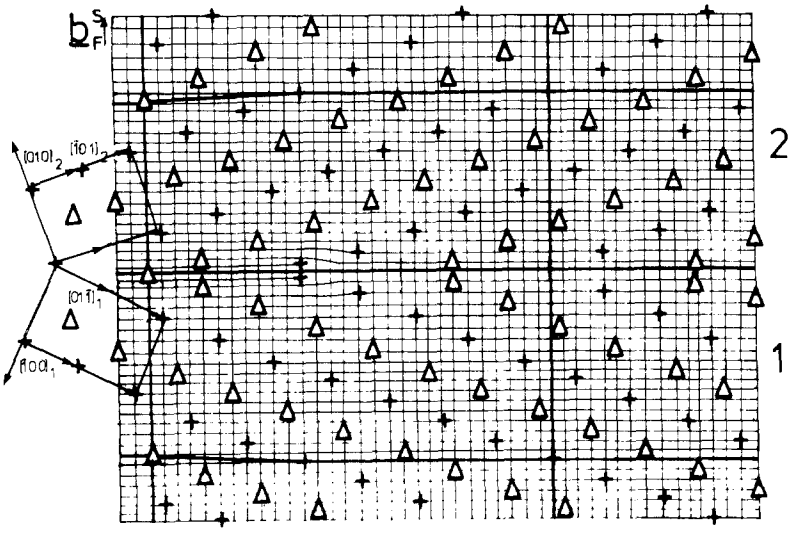

(b)

Figure 7 The DSC lattice for the $\Sigma = 9$ boundary used to illustrate (a) the boundary step, and boundary migration, accompanying the passage of a glissile $\mathbf{b}_1$ type DSC dislocation across a $(1\,2\,\bar{2})_1/(\bar{2}\,\bar{1}\,2)_2$ boundary plane, and (b) the formation of a sessile edge, with no boundary step, caused by the same dislocation in the $(4\,\bar{1}\,1)_1/(\bar{1}\,4\,1)_2$ boundary plane. The Δ and + symbols represent the ABA... stacking sequence of the $\{2\,2\,0\}$ plane.

interpretation is consistent with electron microscope observations which show significant changes in image contrast of lattice dislocations trapped in grain boundaries upon heating. Consideration of the motion of grain boundary dislocations leads to a description of the migration of coincidence related grain boundaries as a form of twinning, but with the difference that, in all but special

Figure 6 Sequence of micrographs taken during heating of the boundary. After 60 sec at 575° C, note rotation of boundary plane, and absorption of leading dislocation in the pile-up from lattice 1 (see Fig. 5a) whose faint residual image is arrowed: (a) $\mathbf{g} = \bar{1}\,1\,1_1$ BF; (b) $\mathbf{g} = 1\,\bar{1}\,\bar{1}_1$ DF. After 2 min at 650° C, the crystal lattice dislocation from crystal 1 appears to leave at least two resolvable grain boundary dislocations (arrowed): (c) $\mathbf{g} = 1\,\bar{1}\,\bar{1}_1$ DF; (d) $\mathbf{g} = 2\,0\,0_2$ DF. After 2 min at 680° C, showing the residual image of the $\mathbf{b}_1$ type DSC dislocations: (e) $\mathbf{g} = 2\,0\,0_2$ BF; (f) $\mathbf{g} = \bar{2}\,0\,0_2$ DF. Scale marker is 1000 A.

cases, the process is diffusion limited, and hence temperature dependent. A particular feature of the model is that a single thermally activated atomic jump leads to a group of atoms changing from positions in one grain to positions in the other.

References

1. P. H. PUMPHREY and H. GLEITER, *Phil. Mag.* **30** (1974) 593.
2. *Idem, ibid.* **32** (1975) 881.
3. R. C. POND and D. A. SMITH, Grain Boundaries 1976, A10, Institution of Metallurgists (London) Series 3, 901–76–Y.
4. *Idem, Phil. Mag.* **36** (1977) 353.
5. A. F. SMITH and G. B. GIBBS, *Metal Sci. J.* **3** (1969) 93.
6. R. C. POND and D. A. SMITH, 3rd International Conference on Textures, Cambridge (Metals Soc., London, 1975) p. 132.
7. H. GRIMMER, W. BOLLMANN and D. H. WARRINGTON, *Acta Cryst.* **A30** (1974) 197.
8. W. BOLLMANN, "Crystal Defects and Crystalline Interfaces" (Springer–Verlag, Berlin, (1970) p. 148.
9. D. H. WARRINGTON and W. BOLLMANN, *Phil. Mag.* **25** (1972) 1195.
10. A. R. THÓLEN, *Phys. Stat. Sol. (a)* **2** (1970) 537.
11. F. HAESSNER, *J. Phys.* **36** (1975) C4.

Received 31 January and accepted 18 April 1978.